

# Ion transmission in an electrospray ionization-mass spectrometry interface using an S-lens

Yihui Yan | Lucas Schmitt | Anastasiya Khramchenkova | Jozef Lengyel 

Chair of Physical Chemistry, TUM School of Natural Sciences, Technical University of Munich, Garching, Germany

## Correspondence

Jozef Lengyel, TUM School of Natural Sciences, Technical University of Munich, Lichtenbergstr. 4, 85748 Garching, Germany.  
Email: [jozef.lengyel@tum.de](mailto:jozef.lengyel@tum.de)

## Funding information

Deutsche Forschungsgemeinschaft,  
Grant/Award Number: LE 4583/1-1

## Abstract

We present the design and performance of an in-house built electrospray ionization-mass spectrometry (ESI-MS) interface equipped with an S-lens ion guide. The ion source was designed specifically for our ion beam experiments to investigate the chemical reactivity and deposition of the clusters and nanoparticles. It includes standard ESI-MS interface components, such as nanoelectrospray, ion transfer capillary, and the S-lens. A custom design enables systematic optimization of all relevant factors influencing ion formation and transfer through the interface. By varying the ESI voltage and flow rate, we determined the optimal operating conditions for selected silica emitters. A comparison of the pulled silica emitters with different tip inner diameters reveals that the total ion current is highest for the largest tip, whereas a tip with the smallest diameter exhibited the highest transmission efficiency through the ESI-MS interface. Ion transmission through the transfer capillary is strongly limited by its length, but the loss of ions can be reduced by increasing the capillary voltage and temperature. The S-lens was characterized over a wide range of RF frequencies and amplitudes. Maximum ion current was detected at RF amplitudes greater than 50 V peak-to-peak (p/p) and frequencies above 750 kHz, with a stable ion transmission region of about 20%. A factor of 2.6 increase in total ion current is observed for 650 kHz as RF amplitudes reach 400 V p/p. Higher RF amplitudes also focus the ions into a narrow beam, which mitigates their losses when passing through the ion guide.

## KEY WORDS

ion trajectory simulation, ion transfer, nanoelectrospray, RF focusing, stacked ring ion guide

## 1 | INTRODUCTION

Electrospray ionization mass spectrometry (ESI-MS) has become a routine technique in modern analytical and clinical laboratories due to its ability in detecting and quantifying individual compounds from complex samples with high sensitivity. It can be applied to a wide range of analytes, from small molecules through polymers to proteins with very high molecular masses.<sup>1,2</sup> Furthermore, the direct coupling of ESI-MS with separation techniques such as liquid chromatography

and capillary electrophoresis facilitates a more comprehensive and selective analysis of complex environmental and biological samples.<sup>3–6</sup>

The key feature of the technique lies in transferring preformed ions from solution directly to the gas phase. A sample is ionized at atmospheric pressure in the ion source and then transferred into a high vacuum region of the mass spectrometer by orifice or inlet capillary.<sup>7,8</sup> This requires efficient ion transmission and reduced residual gas flow through the ESI-MS interface, as gas flow strongly

This is an open access article under the terms of the [Creative Commons Attribution](#) License, which permits use, distribution and reproduction in any medium, provided the original work is properly cited.

© 2023 The Authors. *Journal of Mass Spectrometry* published by John Wiley & Sons Ltd.

influences ion motion and may also result in the loss of analyte ions. Sensitivity of mass spectrometers, for example, limit of detection, is therefore significantly affected by the ion transmission at the ESI/MS interface. There has been extensive research to determine the factors that contribute to the formation of charged droplets, such as solvent composition, the use of volatile buffers, flow rates, material and geometry of the emitter, spray voltage, auxiliary gas, and so forth.<sup>9–13</sup> Understanding how these parameters affect droplet formation led to the remarkable development of nanoelectrospray (nanoESI),<sup>14</sup> which dramatically increased the sensitivity of mass spectrometers. A nanoESI source operating at a flow rate of tens of nL/min generates much smaller droplets than a conventional ESI system. The efficient evaporation of analyte ions in small droplets is greatly enhanced due to their high surface-to-volume ratio and even requires lower electric fields for stable ESI spray.<sup>14–16</sup>

The sprayed charged particles generated at ambient conditions are then pulled into an ion transfer capillary to the entrance vacuum chamber by a pressure gradient. Transfer capillaries are elongated cylindrical tubes heated to facilitate ion desolvation. In general, increased capillary length is associated with decreased ion transmission.<sup>17</sup> A number of simulation studies have described the dynamics of gas flow in these capillaries.<sup>18–22</sup> Standard transfer capillaries may transmit up to 50% of ions,<sup>17,23–25</sup> which has been improved even further by modifying the capillary geometry.<sup>26,27</sup> Ions from the ion transfer capillary enter the first vacuum stage operating typically at several hundred Pa. This is one of the most critical phases owing to the free jet expansion of the gas flow, causing the beam to spread radially and accelerate to sonic or even supersonic velocities.<sup>20</sup> Another crucial consequence of the relatively high pressure in the first chamber is the high number of collisions, making challenging to control the ion trajectories. In order to create a directed gas flow, these ions are usually focused by stacked-ring ion guides, which are better suited for operation at high background pressure than rod-based multipoles (e.g., hexapole or octupole). The most prominent example of such an ion guide is undoubtedly an ion funnel, which focuses an ion beam using a series of stacked ring electrodes with decreasing inner diameter.<sup>28–38</sup> With a radiofrequency (RF) voltage applied to the funnel, ions are radially pushed toward the centerline (adjacent rings are supplied with RF signals with a 180° phase shift) while a potential gradient pushes them axially toward the narrow exit slit. Some stacked-ring ion guides are being used in commercial instruments, such as StepWave (Waters)—a dual stage conjoined ion guide with a DC offset potential to propel ions from the lower to the upper stage.<sup>39</sup> In 2009, the Thermo Scientific LTQ ion trap instruments were equipped with a new type of stacked-ring ion guide, called S-lens.<sup>40</sup> In contrast to the ion funnel, the S-lens has a much simpler construction that operates as an RF only device without requiring a DC offset. It consists of two sequential sets of progressively-spaced flat ring electrodes to which RF voltages are applied, with opposite phases on adjacent rings. In the first set, rings with a larger inner diameter capture the entire ion cloud from expansion, while in the second set, rings with a smaller inner diameter focus the ion beam and guide it through an exit lens.<sup>40–42</sup> A fixed RF voltage of 650 kHz is applied to the electrodes,

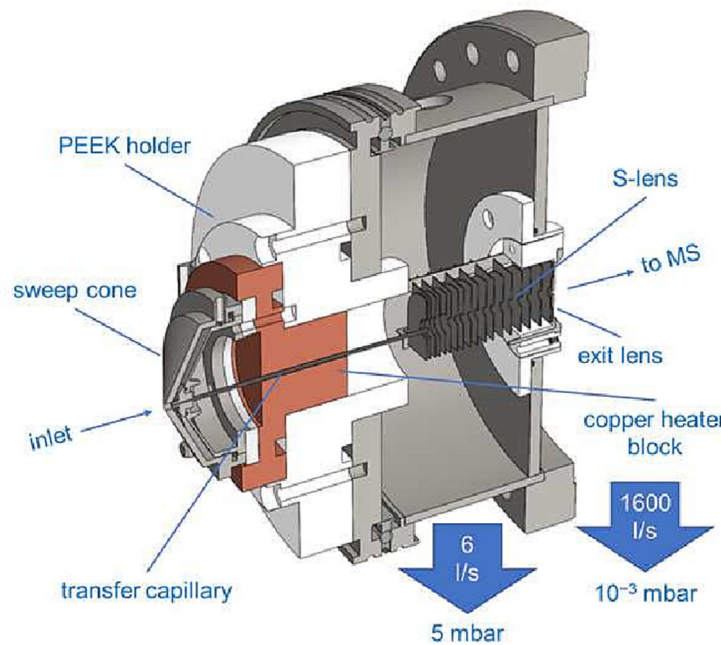
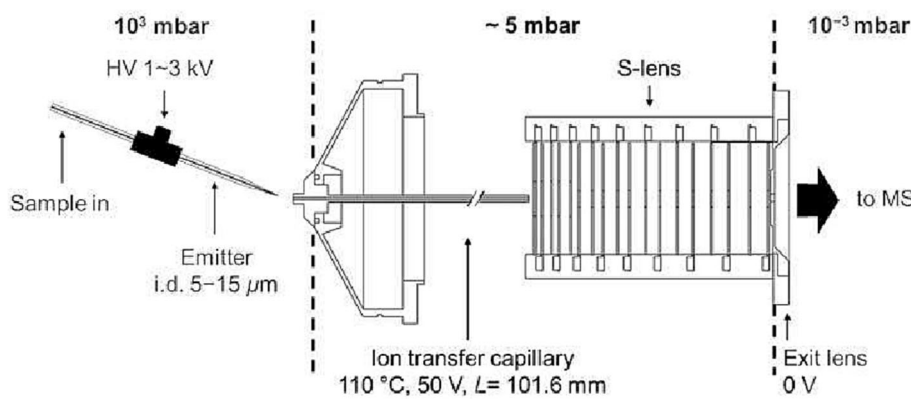
and ion transmission of compounds of different masses is tuned by the RF amplitude, which can be as high as 300 V (peak-to-peak, p/p). The S-lens increases the current by a factor of five, compared to the capillary-skimmer interface used in earlier generation LTQ mass spectrometers.<sup>43</sup>

In the present study, we designed an ESI-MS interface, which comprises the NanoESI ion source, ion transfer capillary, and S-lens ion guide. Our design enables a comprehensive and systematic exploration of factors influencing ion formation and transfer efficiency for each component. By plotting correlations between these factors, we can identify optimal operating conditions for achieving a stable ion beam with maximum ion current. First we compare ion intensities generated using different types of NanoESI emitters as a function of flow rates and electrospray voltages. The second step is to investigate how the temperature and capillary voltage affect the ion transmission through the ion transfer capillary. As a final step, we investigate whether RF-voltage and RF-amplitude variations can enhance ion transmission through the S-lens.

## 2 | EXPERIMENT

The experiments were performed on our custom-made ESI ion source with the PST-MS-Thermo (Phoenix S&T) single column source and an ESI/MS interface with the S-lens, shown schematically in Figure 1. The ion source is a hybrid design comprising both custom-made and commercially available components. It was specifically designed to be integrated with our in-house built experimental setups dedicated to studying gas-phase cluster reactivity and surface deposition.<sup>44,45</sup> Ions were generated by electrospray ionization in a positive mode using a 0.1 mM rhodamine B dissolved in a 1:1 (vol/vol) solution of MeOH:H<sub>2</sub>O, containing a 2% (by volume) acetic acid buffer. The flow rate of the analyte solution was controlled by a syringe pump (New Era, NE-1002X), varying between 10 and 500 nL/min. The solution was then sprayed by the emitter. A total of four different emitters were tested in this experiment, namely, pulled silica emitters (CoAnn Technologies) with inner tip diameters of 5, 7, and 15 μm and quartz silica emitter (Sharp Singularity emitter, Fosiliontech) of 10 μm constant i.d. A voltage in a range of 1.0–3.0 kV was applied to the emitter to determine the best performance in achieving stable spray conditions and maximum ion yield. Sufficient droplet desolvation was accomplished by using a flow of dry nitrogen around the emitter. Ions sprayed at ambient conditions were transferred into a vacuum stage of the source chamber through a 101.6 mm long transfer capillary (LTQ, Thermo Scientific) with an inner diameter of 0.58 mm. The capillary was mounted on a copper block, which can be resistively heated up to 120° C and supplied with a voltage to efficiently pull ions through the capillary. Ions enter the first pumping stage with a backup pressure of 5 mbar, in which they are focused into an ion beam by the S-lens. Approximately 20% of the ions pass through the exit lens with an aperture 2 mm in diameter located after the S-lens that separates the next differentially pumped vacuum stage at a backup pressure of  $5.0 \times 10^{-3}$  mbar.

**FIGURE 1** Schematic drawing of the ESI/MS interface.



Our main focus was on designing a new source chamber with two differential pumping stages for efficient pressure reduction, combined with an ion guide to efficiently focus the ion beam in order to maximize transmission through these pumping stages. This was accomplished by mounting the standard S-lens assembly (Thermo Scientific). The RF voltage applied to the S-lens is generated by RF generators that are capable of operating in two modes. Following the commercial instrumentation, the first generator (RFG50, CGC Instruments) runs at a fixed output frequency of 0.65 MHz with a maximum peak-to-peak amplitude of 400 V and generates a sine-shaped RF signal.<sup>46</sup> The second RF generator (developed at TUM Physics) provides a square wave signal at a variable output frequency of 0.5–10 MHz with a maximum amplitude of 100 V p/p.

The ion transmission measurements were carried out by measuring the total ion current using a picoammeter (Keithley, Model No. 6485). The total ion current measurements, however, do not provide a complete picture of the transmission efficiency of an ESI interface because ions of interest are indistinguishable from solvent ions, charged droplets, and particles. To track the formation of ions in the emitters and their transport through the transfer capillary, the ion

current was measured by replacing the S-lens with a stainless steel disk, which acts as a charge collector. In order to prevent ion loss, the metal disk is placed in close proximity to the exit of the transfer capillary ( $\sim 0.8 \text{ cm}$ ). The disk is connected by a BNC coaxial feedthrough to a picoammeter. Likewise, a metal disk in similar arrangement is used to track the ion current after the S-lens. The present values represent an average of 100 consecutive measurements acquired through an in-house coded LabVIEW data acquisition program. Contour plots are used to visually illustrate how the total ion current changes based on two different variables. Data from measurements are represented by intersecting points on these graphs.

### 3 | RESULTS AND DISCUSSION

#### 3.1 | Electrospray emitters and transfer capillary

At first, we examined the formation of ions by electrospray ionization at ambient conditions. We tested the best performance of four different ESI emitters at a wide range of flow rates and ESI voltages. In all

cases, we used the test solution of 0.1 mM rhodamine B sprayed from the ESI emitter, which was positioned with respect to the inlet of the ion transfer capillary for maximum ion current. Our measurements focused on silica emitters of different inner diameters (i.d.), including pulled silica emitters having different capillary and tip i.d. and quartz silica emitters with a constant capillary and tip diameter. For example, the capillary i.d. of a 10  $\mu\text{m}$  pulled silica emitter decreases to 5  $\mu\text{m}$  at the tip. For 20  $\mu\text{m}$  and 50  $\mu\text{m}$  ESI emitters, the tips have i.d. of 7  $\mu\text{m}$  and 15  $\mu\text{m}$ , respectively. The measurement of total ion current on the inlet sweep cone revealed that transfer capillaries with larger diameters produce a greater amount of ions. Specifically, the highest ion currents were observed with pulled silica emitters with a tip inner diameter of 15  $\mu\text{m}$ . The ion current was found to be strongly dependent on the flow rate, increasing gradually from 35 nA at 10 nL/min to 180 nA at 500 nL/min. The pulled silica emitter with a tip inner diameter of 7  $\mu\text{m}$  yielded an ion current ranging from 50 to 80 nA for within 10–500 nL/min. It is then not surprising than the lowest ion current was measured for a 5  $\mu\text{m}$  emitter. Unlike the larger capillaries, the 5  $\mu\text{m}$  capillary did not exhibit any significant dependence on the flow rate and instead showed a relatively constant ion current ranging from 11 to 15 nA. Interestingly, the quartz emitter of 10  $\mu\text{m}$  diameter showed a slight increase in ion current from 14 to 24 nA, but the absolute value was much lower than reported for pulled silica emitters of similar size. Overall, the observed increase in total ion current with increasing emitter diameter and higher flow rates is attributed to the higher number of ions that can be sprayed to the front of the interface within a given time frame.

However, a substantial loss in ion current is expected when ions pass into the first pumping stage, as only a portion of the spray current sampled into the inlet. By collecting the charge right after the transfer capillary, we measured a maximum total ion current of approximately 0.8 nA for pulled silica emitters with tip i.d. of 7 and 15  $\mu\text{m}$ , which was slightly larger than the maximum total ion current measured for quartz silica with a 10  $\mu\text{m}$  i.d.. A pulled silica emitter with a 5  $\mu\text{m}$  i.d. provided the lowest absolute current of about 0.5 nA. The distance between the ESI emitter and the inlet was the most sensitive parameter, with shorter distances resulting in higher ion current measurements as a larger portion of the sprayed plume being sampled into the instrument. Another significant contribution to the loss of ions occurs on the capillary walls, which is strongly influenced by the length of the transfer capillary. For example, Smith and coworkers have shown that by increasing the capillary length from 13 mm to 64 mm, the ion transmission efficiency can decline from 18% to 2%.<sup>17</sup> Given our 101.6-mm-long transfer capillary, it is then not surprising that only a small amount of current penetrated through the interface into the first pumping stage, about 1% to 4% of the total ion current sprayed from the ESI emitter. By comparing pulled silica emitters, the highest loss in ion current was found for 7 and 15  $\mu\text{m}$  i.d. emitters, whereas transfer efficiency seems to increase threefold for 5  $\mu\text{m}$  i.d. ESI emitter. This clearly indicates that a larger portion of the spray enters the instrument with smaller ESI emitters, thus producing a finer, more compact spray. The larger ESI emitters also produce significantly more ions, which leads to greater space-charge ion losses.

In Figure 2, the ion current is plotted against flow rates and ESI voltages for all four emitters. For the smallest pulled silica emitter (5  $\mu\text{m}$  i.d. tip, 10  $\mu\text{m}$  i.d. capillary, Figure 2A), the ion current is barely observed up to 1.6 kV, likely below the onset potential to generate stable spray. A higher flow rate shifts the onset of an electrospray to 2.0 kV. The shift to higher onset potentials can be attributed to a larger meniscus on the emitter as a result of an increase in flow rate.<sup>47</sup> At flow rates between 10 and 100 nL/min, the total ion current rises gradually with increasing ESI voltage and reaches a maximum of about 0.4 nA at 2.1 kV ESI voltage. Further increase of ESI voltage does not lead to any substantial increase in ion current. As shown in Figure 2A, the highest current is located in a very narrow region at low flow rates. The ESI performance with a 5  $\mu\text{m}$  i.d. tip emitter is most efficient between 2.3 and 2.5 kV for flow rates of 10 to 100 nL/min, which is consistent with the preference for low flow rate ESI experiments.

Compared to the smallest ESI emitter, the pulled silica emitters with a larger tip orifice generated twice as much total ion current and the optimal operation parameters shift to higher flow rates. Figure 2B shows the total ion current measurements for a 7  $\mu\text{m}$  tip i.d. emitter. The maximum ion current is observed at ESI voltages of 2.3–2.5 kV and flow rates between 100 and 200 nL/min. At higher flow rates, the ESI voltage exhibits a very little variation in ion current. Over 200 nL/min, the plume contains larger “micro” droplets, independent of the onset potential, making the spray unstable. In this case, the high flow rate through a very small tip most likely overwhelms the emitter, reducing spray quality even though the total ion current appears to be sufficient. The 15  $\mu\text{m}$  tip i.d. emitter shows a similar trend, resulting in a stronger ion current, which is shifted to higher flow rates with a lower onset potential. The maximum ion current was measured at a potential of 1.8 kV with flow rates around 300 nL/min. As the emitter tip diameter increases, ESI performance for pulled silica emitters of different diameters shifted systematically to higher flow rates and lower onset potentials. For the flow rate dependence, one can imagine that the inner diameter of the emitter tip determines the initial droplet size, that is, a smaller orifice of the emitter reduces the volume of the droplet accumulating at the tip.<sup>48</sup> Therefore, the smallest capillary has a very narrow stability region at low flow rates, in contrast to the larger ones, which have a broader stability region at higher flow rates.

The ion current produced by a quartz silica ESI emitter with a constant 10  $\mu\text{m}$  diameter, shown in Figure 2D, exhibits higher stability than the pulled silica emitters. The best performance is achieved at flow rates of 100–200 nL/min over a wide range of ESI voltages, ranging from 1.6 kV to 2.4 kV. In general, increasing ESI voltage is associated with higher ion currents. Higher flow rates have the opposite effect and decrease ion current.

The ion transport through capillaries is a complex process that is influenced by many factors, including electric forces (either externally by applying electric potential or internally by space charges of the ion cloud), gas flow dynamics, and heating. However, measuring ion current alone cannot account for all of these factors. Hence, our focus is not on describing the fundamentals of ion transmission through

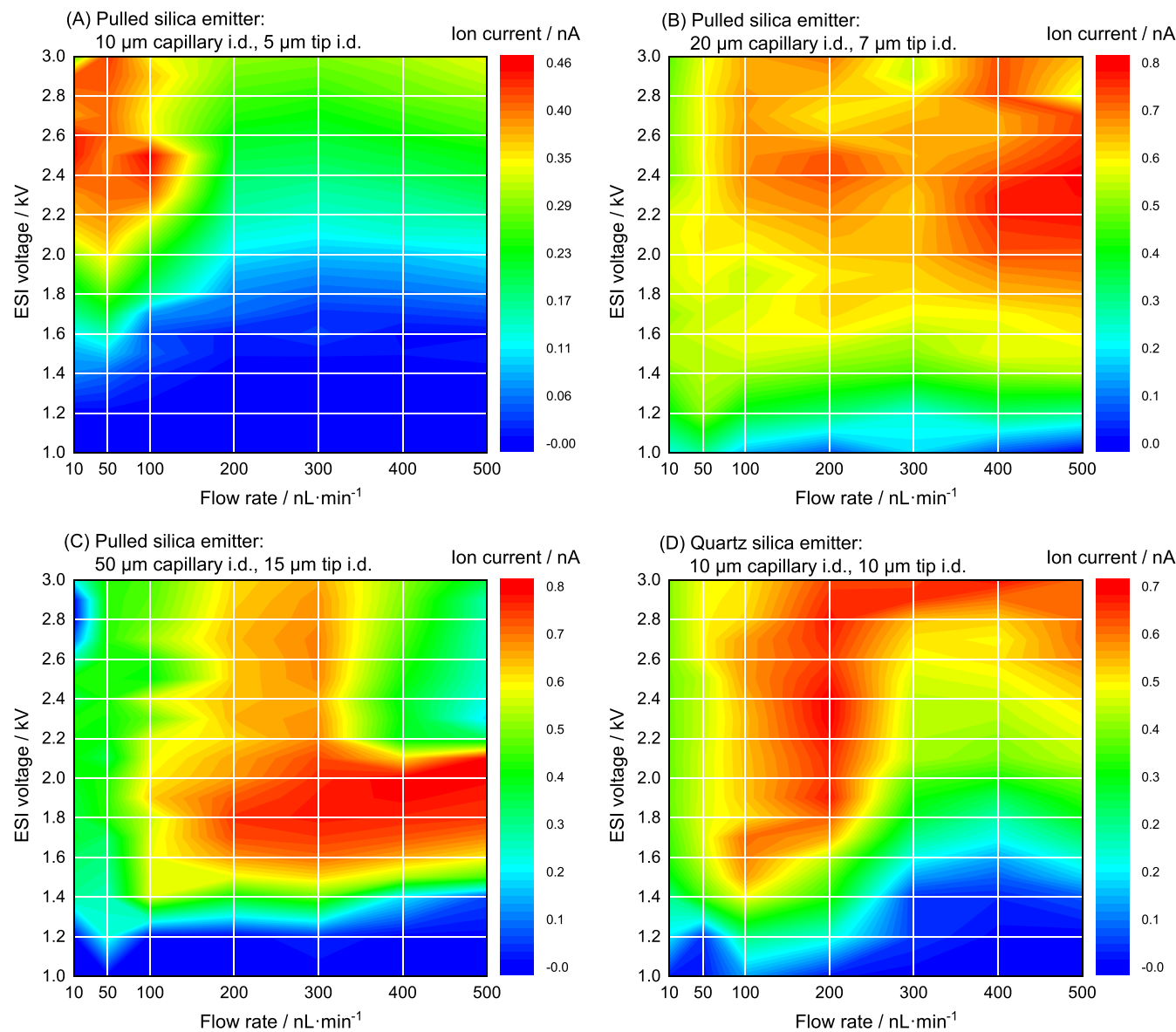


**FIGURE 2** Ion intensities as a function of flow rate and ESI voltage with four different emitters; (A–C) pulled silica emitters with a tip i.d. of 5, 7, and 15 µm (CoAnn Technologies), respectively, (D) quartz silica emitter of 10 µm i.d. (Sharp Singularity emitter, Fossilliontech). A temperature of 110° C and a voltage of 50 V were applied to the transfer capillary.

capillaries, nor on how each effect might affect it, but rather on practical ways of increasing it. In particular, we will explore how an external electric field and heating of the capillary can improve ion transmission, shown in Figure 3.

Applying an electrostatic field to a capillary affects the path of ions, particularly at the entrance and exit. Our measurements show that the most sensitive region is up to 40 V, followed by a plateau with limited ion current changes. On average, the variation in electrostatic field across different temperatures leads to a small increase in ion current by a factor of 1.1–1.2. Increasing the voltage creates a field gradient that could favor ions entering the transfer capillary. Alternatively, an electric gradient between the capillary exit and detector plate might influence the path of charged particles. This contribution, however, does not seem significant, since the applied

electric potential is not sufficient to manipulate the ion trajectory, which is driven rather by the viscous gas flow.<sup>19</sup>

Figure 3 also indicates that the higher capillary temperatures improved the total ion current, with the highest values observed at 110–120° C. However, despite the temperature increase from 30° C to 120° C, ion transmission only increased by an average of 10% across all voltages. While temperature has a minimal effect on the kinetic energy of ions (only about 0.011 eV, for an ideal gas with a mean kinetic energy of  $1.5k_B T$ ), movement of ions in capillaries is determined by gas flow, whose velocity, density, and mobility are greatly affected by temperature. The specific effects of each parameter are discussed in the dedicated literature, which presents detailed simulations of gas flow dynamics supported by mass spectrometry measurements.<sup>18–20,22,26</sup> For example, a heated capillary can

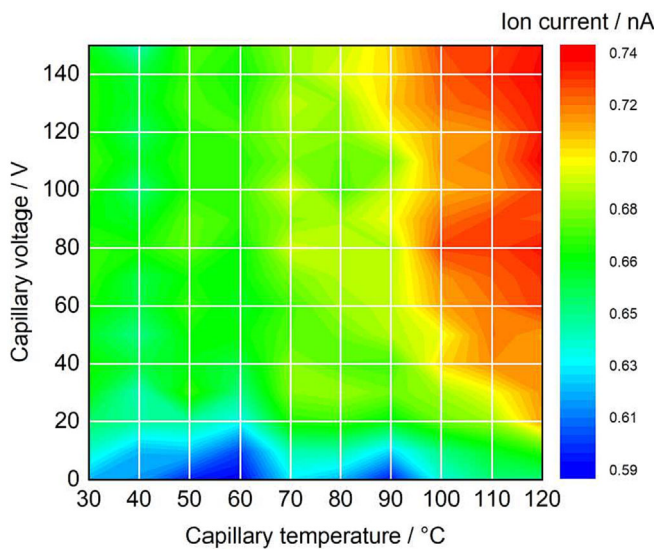


**FIGURE 3** Ion transmission through the transfer capillary at a variety of capillary voltages and temperatures. The quartz silica emitter of 10 µm i.d. were used with ESI voltage of 2.0 kV and a flow rate of 100 nL/min.

experience thermal choking and turbulence transition, both of which affect gas flow dynamics. Thermal choking can accelerate gas flow but reduces the amount of gas transported, whereas the presence of turbulence in laminar flow typically reduces the gas flow.<sup>18</sup> For most capillaries, a turbulent flow is on average 10% slower than a laminar one.<sup>20</sup> Initially, capillary flow is laminar at the inflow and becomes turbulent after a certain distance regardless of temperature. Reiss and coworkers have shown that the occurrence of turbulence can be delayed or even suppressed by heating, which allows for the observed higher transmission rates.<sup>18</sup> Furthermore, water and other solvent molecules can effectively adhere to the inner walls of the inlet capillary, creating multiple layers on the metal surface that can change its surface conductivity.<sup>19</sup> As a result, charged particles and ions entering the capillary can be absorbed in these layers, which may affect the measured total ion current. The number of particles captured depends on the layer thickness, which, in turn, is influenced by the temperature of the capillary and needs to be considered as a potential contribution.

### 3.2 | S-lens

The ions emitted from the transfer capillary entered the S-lens, where an oscillating electric field began to affect their motion. In this case, the ion transmission through the ion guide can be tuned by applying a suitable RF frequency and amplitude. In order to gain information about optimal operation parameters of the S-lens, the ion transmission was characterized across a wide range of RF frequencies and amplitudes. The ion transmission was determined by monitoring ion current on a metal disk located directly after the exit lens and comparing it to the ion current measured at the transfer capillary output.

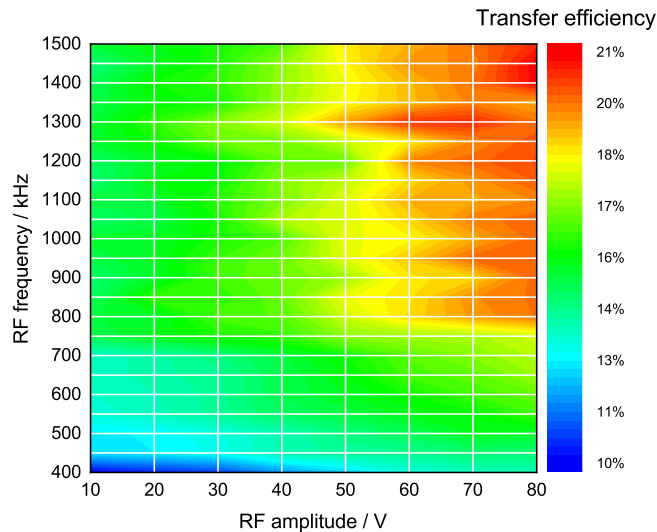


**FIGURE 4** Experimental transmission properties of the S-lens with respect to RF frequency and amplitude. Experiments were conducted using square-wave RF signals.

These experiments with variable RF frequencies employed a square-shaped RF signal applied to the S-lens with the exit lens set to 0 V.

The experimental data, illustrated in Figure 4, shows a strong ion transmission increase at higher RF amplitudes and frequencies. Maximum ion current was detected at RF amplitudes greater than 50 V and frequencies above 750 kHz, and there is a quite broad region of stable ion transmission of around 20%. On the other hand, the lowest ion current was measured at 400–450 kHz with amplitudes up to 50 V, a two-fold decrease compared to the highest intensities. At these lower RF amplitudes, the ion current quickly reached a plateau at about 15% ion transmission, remaining almost constant even when the frequency gradually increased to 1.5 MHz. Overall, changing the frequency from 400 kHz to 1500 kHz resulted in an average ion transmission increase of 6%, whereas varying the RF amplitude from 10 to 80 V increased the transmission by 5%. In line with the experimental findings, ion trajectory simulations performed in SIMION<sup>49</sup> displayed a significant dependence of the ion transmission on RF amplitude and RF frequency. A more detailed description can be found in the Supporting Information. In most cases, optimal S-lens performance could be achieved at RF frequencies of 900–1500 kHz with amplitudes of 40–80 V p/p. The highest transmission efficiency values occurred between 900–1200 kHz and 70–80 V p/p. By reducing the kinetic energies of ions, the optimal RF Range on the S-lens increases and the RF voltages and amplitudes can be even lowered for effective ion transmission (Figure S4 in Supporting Information).

Also, commercial mass spectrometers achieve optimal ion transmission by tuning the RF amplitude on S-lens, which have a fixed RF output frequency of 650 kHz.<sup>50</sup> In general, increased RF amplitudes allow ions of higher mass-to-charge ratio to pass through the ion guide. For example, the TSQ Vantage operates with RF amplitudes up to 300 V p/p, adjusting the amplitude for each ion individually.<sup>50</sup> Figure 5 illustrates the operation of such an S-lens, capable of tuning

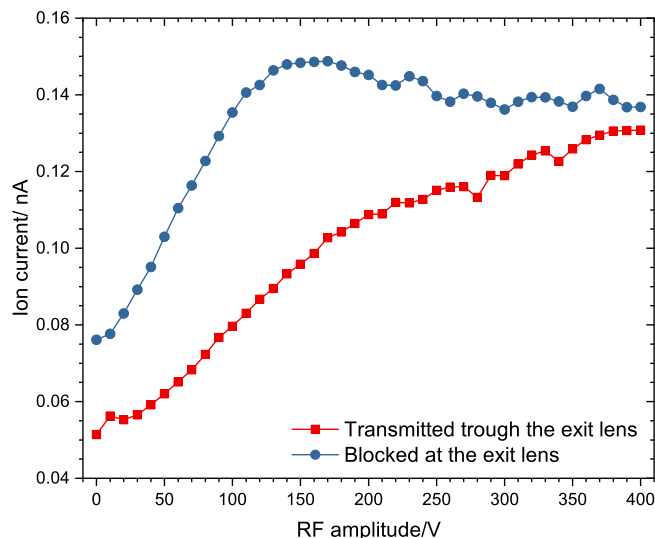


**FIGURE 5** Ion transmission through the S-lens controlled by a sine-wave RF signal with a fixed frequency output of 650 kHz and a variable amplitude of 0 to 400 V p/p. The ions that pass through the S-lens but are blocked by the exit lens are shown as blue circles, whereas ions that pass through the entire ion guide are shown as red squares.

RF amplitudes up to 400 V p/p at a fixed frequency of 650 kHz with a sine-shaped RF signal. It should be noted that the transmission properties of S-lens for sine- and square-wave RF signals exhibited similar characteristics upon measuring total ion currents up to 80 V (Figure S1 in the Supporting Information). Similar observations are reported for rod-based multipoles, whose transmission spectra are nearly identical with respect to the transfer efficiency, apart from a small shift of the maximum toward lower amplitudes for square-wave multipoles.<sup>51–53</sup> In order to illustrate the effect of RF amplitude on ion transmission through the S-lens, we measured the ion current on the exit lens in addition to the ion current on the metal disk located after the S-lens. Ion current measured at the exit lens is caused by ions colliding with the lens, that is, being blocked from traversing the ion guide. On the other hand, increasing ion current measured on the metal disk implies higher ion transmission through the S-lens. In this case, the exit lens was maintained at 0 V, as the application of electric potential would reduce ion transmission (Figure S2 in the Supporting Information).

Ion current measurements conducted at a varying RF amplitude (0–400 V) and a fixed sine-shaped RF frequency of 650 kHz are summarized in Figure 5. The ion current on the metal disk (red) steadily increases with the RF amplitude, whereas the current measured on the exit lens (blue) exhibits two distinct progressions. First, ion current gradually increases until RF amplitude reaches 140 V p/p, due to higher ion transmission through the bulk of the S-lens and more frequent collisions with the exit lens. Upon reaching a maximum of around 0.15 nA at 140–180 V, further increasing the amplitude to even higher values leads to a decrease in ion current down to 0.14 nA at 400 V. Considering the continuously rising ion current values at the metal disk in the same amplitude range (180–400 V), a slight decrease

in ion current on the exit lens suggests that less ions hit the exit lens, while simultaneously more ions pass through the S-lens. This behavior can be explained by the fact that higher RF amplitudes allow for better focusing of the ion beam. The most efficient ion transmission is achieved at the high end of our range, that is, 400 V, when about half of the ions pass through the S-lens.

## 4 | CONCLUSION

We designed the ESI-MS interface equipped with S-lens, consisting of three major components: nanoelectrospray source, ion transfer capillary, and S-lens stacked-ring ion guide. Each of them was optimized step-by-step for optimal operation by varying adjustable factors influencing ion formation and transmission through the interface. While the ion source was designed for a specific experimental setup, the results can be generalized to commercial instruments. Major conclusions can be summarized as follows:

- The influence of ESI voltage and flow rate was investigated for ion formation in different silica ESI emitters. Quartz silica emitters with constant i.d. exhibited better spray stability over time than pulled silica emitters, whose tip i.d. are smaller than i.d. of their capillaries. Ion current measurement of pulled silica emitters revealed a positive correlation between tip diameter and ion current. For example, a 15 μm tip i.d. emitter had a nearly twofold higher total ion current in the first pumping stage than one with a 5 μm diameter. In contrast, the 5 μm tip i.d. emitter transmits ions more efficiently through the ESI-MS interface than the 15 μm counterpart by a factor of three. It seems that the cone jet of the smaller ESI emitter is more compact, resulting in a reduced loss of ions when transferred into a vacuum chamber. Also, transmission through the transfer capillary can be maximized by adjusting the capillary voltage and temperature. It is important to note that the performance of commercial ESI sources can vary from one to another due to different designs and geometries. Nevertheless, all these correlations can be used as a starting point for optimizing the performance of commercial ESI systems.
- The ion transmission through the S-lens was tested at various RF frequencies and amplitudes. We did not observe differences in transmission properties between sine-shaped and square-wave RF signals on the S-lens. Maximum ion current was detected at RF amplitudes greater than 50 V p/p and frequencies above 750 kHz, with a stable ion transmission region of about 20%. Furthermore, ion motion simulations indicated a strong positive correlation between RF amplitude and ion current. It was confirmed experimentally with an over 2.5-fold increase in total ion current at amplitudes of 400 V p/p. Our experiments further revealed that the application of higher RF amplitudes is essential for narrowing the ion beam in order to minimize ion losses at the exit lens. Overall, understanding the impact of each electric field parameter on ion motion is essential to optimize the performance of the ion guide in mass spectrometry. This knowledge is particularly useful

for commercial instruments utilizing the S-lens, as they usually provide limited access to the hardware.

## ACKNOWLEDGMENTS

This study was funded by the Deutsche Forschungsgemeinschaft (DFG, German Research Foundation; Project LE 4583/1-1) within the Emmy Noether program. We thank Andreas Walz for providing us with a modular RF generator and for numerous fruitful discussions. Open Access funding enabled and organized by Projekt DEAL.

## DATA AVAILABILITY STATEMENT

All of the presented data are available from the corresponding author upon request.

## ORCID

Jozef Lengyel  <https://orcid.org/0000-0002-1971-2783>

## REFERENCES

1. Fenn JB, Mann M, Meng CK, Wong SF, Whitehouse CM. Electrospray ionization—principles and practice. *Mass Spectrom Rev.* 1990;9(1):37-70.
2. Gross JH. *Mass Spectrometry: A Textbook*. 3rd ed. Cham, Switzerland: Springer; 2017.
3. Angel TE, Aryal UK, Hengel SM, et al. Mass spectrometry-based proteomics: existing capabilities and future directions. *Chem Soc Rev.* 2012;41(10):3912-3928.
4. Beccaria M, Cabooter D. Current developments in LC-MS for pharmaceutical analysis. *Analyst*. 2020;145(4):1129-1157.
5. Bowen BP, Northen TR. Dealing with the unknown: metabolomics and metabolite atlases. *J Am Soc Mass Spectrom.* 2010;21(9):1471-1476.
6. Wu H, Tang K. Highly sensitive and robust capillary electrophoresis-electrospray ionization-mass spectrometry: interfaces, preconcentration techniques and applications. *Rev Anal Chem.* 2020;39(1):45-55.
7. Bruins AP. Mass spectrometry with ion sources operating at atmospheric pressure. *Mass Spectrom Rev.* 1991;10(1):53-77.
8. Whitehouse CM, Dreyer RN, Yamashita M, Fenn JB. Electrospray interface for liquid chromatographs and mass spectrometers. *Anal Chem.* 1985;57(3):675-679.
9. Kruve A. Influence of mobile phase, source parameters and source type on electrospray ionization efficiency in negative ion mode. *J Mass Spectrom.* 2016;51(8):596-601.
10. Kruve A, Kaupmees K. Predicting ESI/MS signal change for anions in different solvents. *Anal Chem.* 2017;89(9):5079-5086.
11. Oss M, Kruve A, Herodes K, Leito I. Electrospray ionization efficiency scale of organic compounds. *Anal Chem.* 2010;82(7):2865-2872.
12. Reschke BR, Timperman AT. A study of electrospray ionization emitters with differing geometries with respect to flow rate and electrospray voltage. *J Am Soc Mass Spectrom.* 2011;22(12):2115-2124.
13. Schmidt A, Karas M, Dülcks T. Effect of different solution flow rates on analyte ion signals in nano-ESI MS, or: when does ESI turn into nano-ESI? *J Am Soc Mass Spectrom.* 2003;14(5):492-500.
14. Wilm MS, Mann M. Electrospray and Taylor-Cone theory, Dole's beam of macromolecules at last? *Int J Mass Spectrom Ion Process.* 1994;136(2-3):167-180.
15. Jurasic R, Dülcks T, Karas M. Nanoelectrospray—more than just a minimized-flow electrospray ionization source. *J Am Soc Mass Spectrom.* 1999;10(4):300-308.
16. Wilm MS, Mann M. Analytical properties of the nanoelectrospray ion source. *Anal Chem.* 1996;68(1):1-8.
17. Page JS, Marginean I, Baker ES, Kelly RT, Tang K, Smith RD. Biases in ion transmission through an electrospray ionization-mass spectrometry capillary inlet. *J Am Soc Mass Spectrom.* 2009;20(12):2265-2272.
18. Bernier L, Pinfold H, Pauly M, Rauschenbach S, Reiss J. Gas flow and ion transfer in heated ESI capillary interfaces. *J Am Soc Mass Spectrom.* 2018;29(4):761-773.
19. Derpmann V, Müller D, Haack A, Wißdorf W, Kersten H, Benter T. Charging effects in inlet capillaries. *J Am Soc Mass Spectrom.* 2022;33(9):1678-1691.
20. Gimelshein N, Gimelshein S, Lilly T, Moskovets E. Numerical modeling of ion transport in an ESI-MS system. *J Am Soc Mass Spectrom.* 2014;25(5):820-831.
21. Skoblin M, Chudinov A, Soulimenkov I, Brusov V, Kozlovskiy V. Gas flow in the capillary of the atmosphere-to-vacuum interface of mass spectrometers. *J Am Soc Mass Spectrom.* 2017;28(10):2132-2142.
22. Wißdorf W, Müller D, Brachthäuser Y, et al. Gas flow dynamics in inlet capillaries: evidence for non laminar conditions. *J Am Soc Mass Spectrom.* 2016;27(9):1550-1563.
23. Fomina NS, Kretinina AV, Masyukevich SV, et al. Transport of ions and charged droplets from the atmospheric region into a gas dynamic interface. *J Anal Chem.* 2013;68(13):1151-1157.
24. Lin B, Sunner J. Ion transport by viscous gas flow through capillaries. *J Am Soc Mass Spectrom.* 1994;5(10):873-885.
25. Page JS, Kelly RT, Tang K, Smith RD. Ionization and transmission efficiency in an electrospray ionization-mass spectrometry interface. *J Am Soc Mass Spectrom.* 2007;18(9):1582-1590.
26. Bernier L, Taesch M, Rauschenbach S, Reiss J. Transfer conditions and transmission bias in capillaries of vacuum interfaces. *Int J Mass Spectrom.* 2020;447:116239.
27. Pauly M, Sroka M, Reiss J, et al. A hydrodynamically optimized nano-electrospray ionization source and vacuum interface. *Analyst*. 2014;139(8):1856-1867.
28. Anthony SN, Shinholt DL, Jarrold MF. A simple electrospray interface based on a DC ion carpet. *Int J Mass Spectrom.* 2014;371:1-7.
29. Cox JT, Marginean I, Smith RD, Tang K. On the ionization and ion transmission efficiencies of different ESI-MS interfaces. *J Am Soc Mass Spectrom.* 2015;26(1):55-62.
30. Julian RR, Mabbett SR, Jarrold MF. Ion funnels for the masses: experiments and simulations with a simplified ion funnel. *J Am Soc Mass Spectrom.* 2005;16(10):1708-1712.
31. Kelly RT, Tolmachev AV, Page JS, Tang K, Smith RD. The ion funnel: theory, implementations, and applications. *Mass Spectrom Rev.* 2010;29(2):294-312.
32. Kim T, Tang K, Udseth HR, Smith RD. A multicapillary inlet jet disruption electrodynami ion funnel interface for improved sensitivity using atmospheric pressure ion sources. *Anal Chem.* 2001;73(17):4162-4170.
33. Page JS, Tolmachev AV, Tang K, Smith RD. Variable low-mass filtering using an electrodynami ion funnel. *J Mass Spectrom.* 2007;40(9):1215-1222.
34. Shaffer SA, Prior DC, Anderson GA, Udseth HR, Smith RD. An ion funnel interface for improved ion focusing and sensitivity using electrospray ionization mass spectrometry. *Anal Chem.* 1998;70(19):4111-4119.
35. Shaffer SA, Tang K, Anderson GA, Prior DC, Udseth HR, Smith RD. A novel ion funnel for focusing ions at elevated pressure using electrospray ionization mass spectrometry. *Rapid Commun Mass Spectrom.* 1997;11(16):1813-1817.
36. Shaffer SA, Tolmachev A, Prior DC, Anderson GA, Udseth HR, Smith RD. Characterization of an improved electrodynami ion funnel interface for electrospray ionization mass spectrometry. *Anal Chem.* 1999;71(15):2957-2964.
37. Tang K, Shvartsburg AA, Lee H-N, et al. High-sensitivity ion mobility spectrometry/mass spectrometry using electrodynami ion funnel interfaces. *Anal Chem.* 2005;77(10):3330-3339.

38. Tolmachev AV, Udseth HR, Smith RD. Charge capacity limitations of radio frequency ion guides in their use for improved ion accumulation and trapping in mass spectrometry. *Anal Chem*. 2000;72(5):970-978.
39. Giles K, Gordon D. A new conjoined RF ion guide for enhanced ion transmission. In: Proc. 58th ASMS Conf. Mass Spectrometry and Allied Topics; 2010. Waters Application Note 2010: No. 720003606EN:15.
40. Olsen JV, Schwartz JC, Griep-Raming J, et al. A dual pressure linear ion trap orbitrap instrument with very high sequencing speed. *Mol Cell Proteomics*. 2009;8(12):2759-2769.
41. Michalski A, Damoc E, Hauschild JP, et al. Mass spectrometry-based proteomics using q-exactive, a high-performance benchtop quadrupole orbitrap mass spectrometer. *Mol Cell Proteomics*. 2011;10(9): M111.011015.
42. Second TP, Blethow JD, Schwartz JC, et al. Dual-pressure linear ion trap mass spectrometer improving the analysis of complex protein mixtures. *Anal Chem*. 2009;81(18):7757-7765.
43. Eliuk S, Makarov A. Evolution of orbitrap mass spectrometry instrumentation. *Annu Rev Anal Chem*. 2015;8:61-80.
44. Heiz U, Vanolli F, Trento L, Schneider WD. Chemical reactivity of size-selected supported clusters: An experimental setup. *Rev Sci Instrum*. 1997;68(5):1986.
45. Neuwirth D, Eckhard JF, Lange K, et al. Using controlled ion extraction to combine a ring electrode trap with a reflectron time-of-flight mass spectrometer. *Int J Mass Spectrom*. 2015;387:8-15.
46. Cermak I. Compact radio-frequency power supply for ion and particle guides and traps. *Rev Sci Instrum*. 2005;76(6):63302.
47. Wu X, Oleschuk RD, Cann NM. Characterization of microstructured fibre emitters: In pursuit of improved nano electrospray ionization performance. *Analyst*. 2012;137(18):4150-4161.
48. De La Mora JF, Loscertales IG. The current emitted by highly conducting taylor cones. *J Fluid Mech*. 1994;260:155-184.
49. Dahl DA. Simion for the personal computer in reflection. *Int J Mass Spectrom*. 2000;200(1-3):3-25.
50. TSQ series. hardware manual. Tech. Rep. 70111-97163 Revision D, Thermo Fisher Scientific Inc.; 2010.
51. Brabeck GF, Reilly PTA. Mapping ion stability in digitally driven ion traps and guides. *Int J Mass Spectrom*. 2014;364:1-8.
52. Shinholt DL, Anthony SN, Alexander AW, Draper BE, Jarrold MF. A frequency and amplitude scanned quadrupole mass filter for the analysis of high m/z ions. *Rev Sci Instrum*. 2014;85(11):113109.
53. Walz A, Stoiber K, Huettig A, Schlichting H, Barth JV. Navigate flying molecular elephants safely to the ground: mass-selective soft landing up to the mega-dalton range by electrospray controlled ion-beam deposition. *Anal Chem*. 2022;94(22):7767-7778.

## SUPPORTING INFORMATION

Additional supporting information can be found online in the Supporting Information section at the end of this article.

**How to cite this article:** Yan Y, Schmitt L, Khramchenkova A, Lengyel J. Ion transmission in an electrospray ionization-mass spectrometry interface using an S-lens. *J Mass Spectrom*. 2023; 58(7):e4955. doi:[10.1002/jms.4955](https://doi.org/10.1002/jms.4955)